Simulation of Semiconductor Processes and Devices 2016
Edited by E. Bär, J. Lorenz, and P. Pichler

Phase-Space Solution of the Subband Boltzmann Transport Equation for Nano-Scale TCAD

Z. Stanojević, M. Karner, O. Baumgartner, HW. Karner, C. Kernstock, H. Demel, and F. Mitterbauer
Global TCAD Solutions GmbH., Bösendorferstraße 1/12, 1010 Vienna, Austria
Email: {z.stanojevic|m.karner|o.baumgartner|hw.karner|c.kernstock}@globaltcad.com

***Abstract*—We present a comprehensive simulation framework for transport modeling in nano-scaled devices based on the solution of the subband Boltzmann transport equation (BTE). The BTE is solved in phase space using a k·p-based electronic structure model and includes all relevant scattering processes. The BTE solver is combined with a conventional drift-diffusion-based simulator using a novel iteration approach. The pairing between BTE, DD, and Poisson results in a flexible toolkit which converges quickly in any mode of operation, allows large-scale parallelization, and to include near-equilibrium transport outside the BTE region, i.e. the contacting regions. The toolkit is commercially available as part of the GTS Nano Device Simulator (NDS). We examine realistic NMOS and PMOS devices, including transport at the microscopic scale and possible numerical approximations.**

I. Introduction

Simulating current 10 nm nodes and future 7 nm and 5 nm nodes requires simulation methods beyond the standard drift-diffusion based approach. A predictive modeling and simulation toolkit is required to face the design challenges for these technology nodes. In this work, we present such a toolkit, which is built around a subband Boltzmann transport equation (BTE) solver combined with a drift-diffusion based device simulator. The subband BTE contains most of the physical information about the device: it is based on an accurate description of the subband structure, includes all relevant scattering processes occurring in semiconductors at room temperature, and accurately covers effects such as quantum resistance and velocity overshoot. The addition of the drift-diffusion based device simulator enhances the flexibility of the whole software package, which we named the GTS Nano Device Simulator (NDS).

II. Simulation Setup

A typical simulation setup is shown in Fig. 1. Here, a nanowire-FET is shown with thinned-down channel and access regions, connected to larger bulk-like contact regions. We solve the subband Boltzmann transport equation (BTE) in the thin region, while leaving the contact regions to the drift-diffusion/density-gradient model.

We use four test devices based on the architecture from Fig. 1 – two NMOS and two PMOS devices, with diameters 5 nm and 7 nm. The device architecture has a metallurgical gate length of 10 nm with 10 nm long access regions on either side. The channel orientation is ⟨110⟩; source and drain dopings are $1 \times 10^{20}\,\mathrm{cm}^{-3}$. The high-$V_{\mathrm{DS}}$ transfer characteristic for all four devices is shown in Fig. 2.

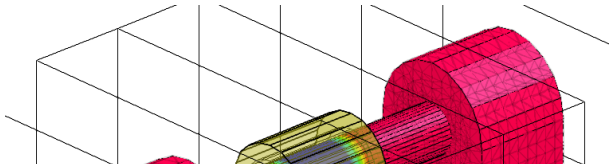

Fig. 1. Nanowire transistor geometry; doping concentration and computational mesh are visible; inset shows the hole concentration calculated by a self-consistent Poisson-DD-BTE simulation, otherwise not obtainable from drift-diffusion/density-gradient model.

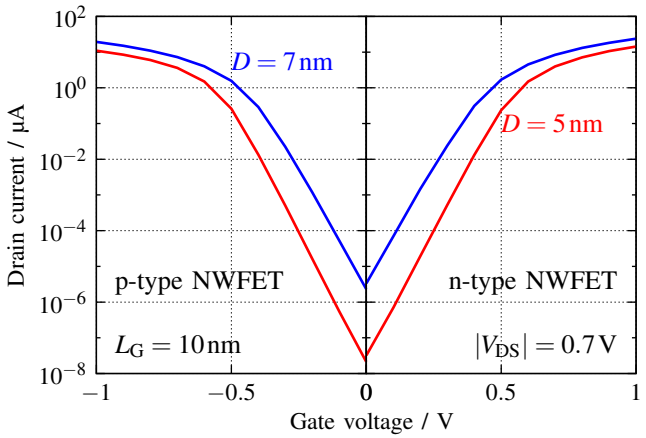

Fig. 2. Transfer characteristics of the test devices at high source-drain bias

III. Subband Boltzmann Transport

The channel and access regions are decomposed into slices perpendicular to the transport direction. On each slice, a **k·p**-based [1, 2] subband structure calculation is performed for every point on a predefined **k**-grid. Using the calculated states and subbands, the scattering models are evaluated producing

978–1–5090–0818–6/16/$31.00 © 2016 IEEE

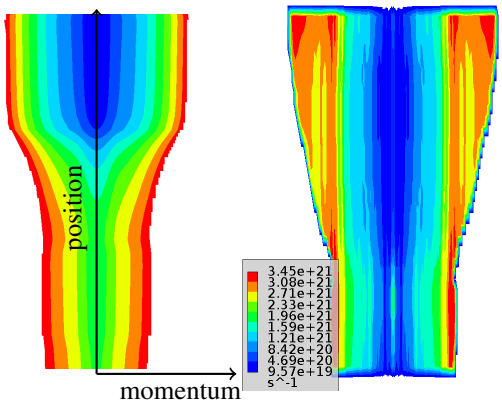

Fig. 3. Left: Phase-space representation of the lowest subband energy for the 7 nm thick NMOS device at $V_{GS} = V_{DS} = 0.7\,V$ (see Fig. 2); Right: Phase-space representation of the scattering rate for the lowest subband of the same device

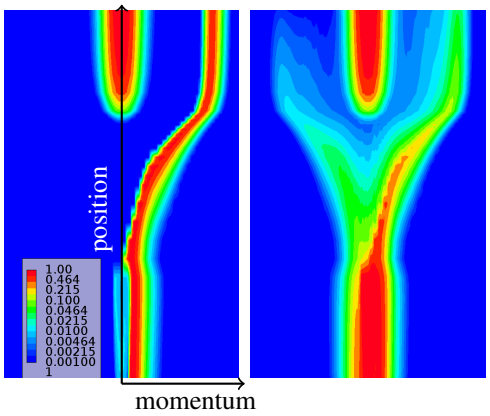

Fig. 4. Ballistic (left) and dissipative (right) electron distribution function in *phase space* for the 7 nm thick NMOS device at $V_{GS} = V_{DS} = 0.7\,V$ (see Fig. 2); the bottom result includes non-polar phonon scattering, interface roughness scattering and impurity scattering.

a scattering operator, i.e. a matrix with the transition rate from each state to any other accessible state on the **k**-grid [3, 4], including inter-subband and inter-valley transitions. The scattering processes included are [5] (i) non-polar acoustic phonons, (ii) non-polar optical phonons for intra and inter-valley scattering, (iii) ionized impurity scattering as well as remote Coulomb scattering, and (iv) interface-roughness scattering [6].

The **k**-grids on each slice are combined to form a $(\mathbf{r},\mathbf{k})$-space, or *phase-space*, which is used to solve the BTE. For a device with a one-dimensional carrier gas, the phase space is a Cartesian product of x, the position along the channel axis, and k, the axial wave-vector, and can be displayed in a two-dimensional plot. Figure 3 shows the the energy dispersion and the scattering rate of the lowest subband in their phase-space representation.

The ballistic probability flux between adjacent states on the phase-space-grid is computed which gives the *free-streaming-operator* of the BTE. One can imagine this procedure as pre-computed Monte-Carlo table: the flux is evaluated by tracing a virtual particle for each state on the **k**-grid of one slice on its ballistic slice, until the particle hits a neighboring slice or the slice where it started.

With the ballistic probability fluxes and the scattering operators for every slice, the BTE can now be solved. A typical phase-space result of the BTE is shown in Fig. 4. The effects of scattering are clearly visible: the particles are partially reflected backwards, visible as mirror image of the ballistic jet, while also undergoing energy relaxation, visible as broadening of the distribution function's high-energy parts.

IV. Coupling with Device Simulator

Electronic structure calculation, scattering models, and BTE solution are implemented as part of the VSP simulator [7, 8]. To calculate a solution which is self-consistent with electrostatics, the device simulator Minimos-NT [9] is used. Minimos-NT first calculates an initial solution, then invokes VSP and passes the electrostatic potential and quasi-Fermi energies to it. VSP solves the BTE and converts the result into an *effective mobility* which reproduces the velocity profile from the BTE solution for the provided quasi-Fermi energy. The method [10] is derived from a similar approach known in Monte-Carlo simulation [11, 12]. Additionally, a quantum correction potential is computed from VSP's result in order to accurately reproduce confinement in Minimos-NT, also known as *self-consistent quantum correction* [10, 13].

Using this method, a converged result can be achieved in a few steps, as shown in Fig. 5. Furthermore, the method is robust enough to start from any bias condition, allowing to parallelize the calculation of the device's characteristics, enabling to calculate them typically below two hours on a cluster with 20 nodes.

V. Discussion

Our approach includes a number of adaptive algorithms, which is also what sets our work apart from that of other authors. Most importantly, the number of calculated subbands is adapted to fill the potential profile up to a certain energy – usually a few $k_B T$ above the top of the barrier (ToB). Looking at the potential in Fig. 5, it becomes obvious that while a few subbands may be enough at ToB to fill 0.1 eV, many more subbands are needed to fill the 0.7 eV potential drop towards the drain.

The quantitative error made by a limited number of subbands can be seen in Figs. 6 and 7. In the ballistic case it is enough to span a sufficiently large energy interval at ToB and keep that number of subbands constant throughout the device, as carriers do not scatter from one subband to another. In the dissipative case the error is much worse, as the absence of high-order subbands yields a reduced scattering rate, thereby leading to an overestimated velocity overshoot.

VI. Conclusion

We present a simulation framework based on the solution of the subband BTE, capable of simulating realistic sub-

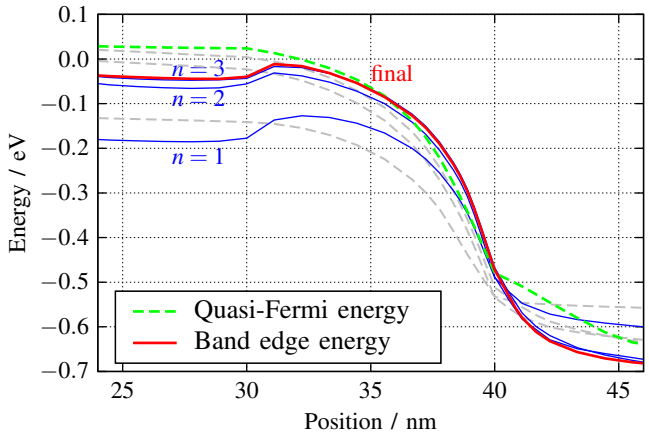

Fig. 5. Convergence behavior of the Poisson-DD-BTE loop; after three iterations the potential and Fermi energy are already close to the converged result.

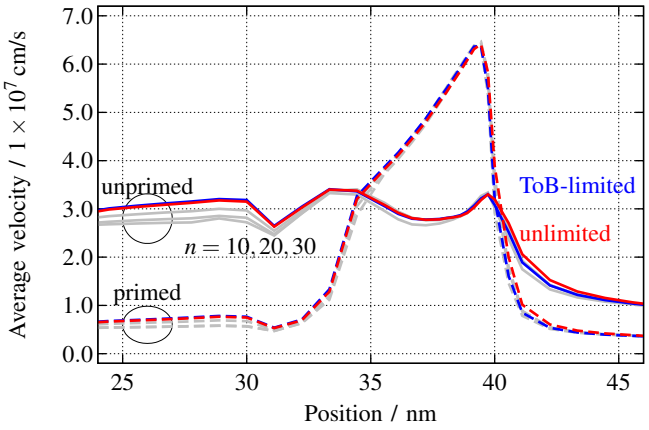

Fig. 6. Average velocity without scattering (ballistic); by setting the number of subbands equal to the number of subbands needed to resolve the distribution function at the top of the barrier (ToB), the ballistic velocity profile is reproduced well. The unprimed valley in a ⟨110⟩-oriented channel is highly non-parabolic; while particle momentum increases during acceleration, the group velocity does not increase monotonically, hence no velocity overshoot can be observed for the unprimed valley.

10 nm devices. The approach is computationally robust and *adaptive*, thus allowing to cast reliable predictions of device performance.

Acknowledgment

This work has been supported by the European Commission through projects MoRV (FP7, Grant no. 619234) and WAY-TOGO FAST (Horizons 2020, Grant no. 662175).

References

[1] J. C. Hensel *et al.*, "Cyclotron Resonance in Uniaxially Stressed Silicon. II. Nature of the Covalent Bond," *Physical Review*, vol. 138, no. 1A, pp. A225–A238, Apr. 1965.

[2] G. Dresselhaus *et al.*, "Cyclotron Resonance of Electrons and Holes in Silicon and Germanium Crystals," *Physical Review*, vol. 98, pp. 368–384, Apr 1955.

[3] Z. Stanojevic *et al.*, "On the Validity of Momentum Relaxation Time in Low-Dimensional Carrier Gases,"

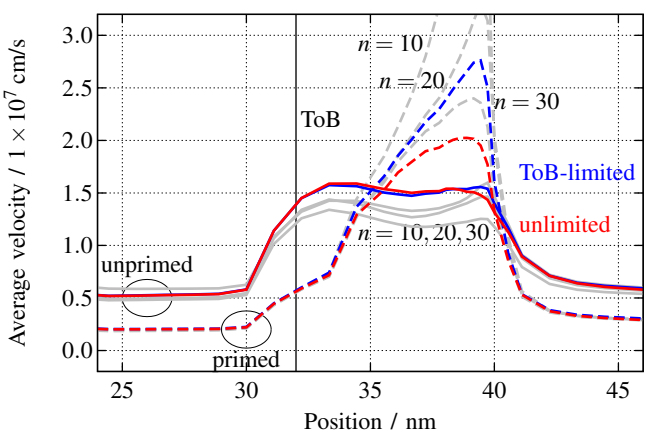

Fig. 7. Average velocity with enabled scattering (dissipative); calculating transport with a fixed number of subbands will either yield too low average velocity due to either having to little populated states, or a too large velocity overshoot because of reduced scattering due to a lack of final states. Setting the number of subbands equal to the number at ToB still overestimates velocity overshoot; the ToB-limited velocity profile begins to diverge from the unlimited one after ToB.

in *International Conference on the Simulation of Semiconductor Processes and Devices (SISPAD)*, 2014, pp. 181–184.

[4] ——, "Advanced Numerical Methods for Semi-Classical Transport Simulation in Ultra-Narrow Channels," in *European Conference on Mathematics in Industry (ECMI)*, 2014.

[5] Z. Stanojević *et al.*, "Consistent low-field mobility modeling for advanced {MOS} devices," *Solid-State Electronics*, no. 0, pp. –, 2015.

[6] Z. Stanojevic *et al.*, "Surface-Roughness-Scattering in Non-Planar Channels – the Role of Band Anisotropy," in *International Conference on the Simulation of Semiconductor Processes and Devices (SISPAD)*, 2013, pp. 352–355.

[7] O. Baumgartner *et al.*, "VSP–a quantum-electronic simulation framework," *J. Comput. Electron.*, 2013.

[8] http://www.globaltcad.com/vsp.

[9] http://www.globaltcad.com/minimos-nt.

[10] Z. Stanojevic *et al.*, "Physical modeling – A new paradigm in device simulation," in *International Electron Device Meeting (IEDM)*, Dec 2015, pp. 5.1.1–5.1.4.

[11] S. Bandyopadhyay *et al.*, "A rigorous technique to couple Monte Carlo and drift-diffusion models for computationally efficient device simulation," *IEEE Transaction on Electron Devices*, vol. 34, no. 2, pp. 392–399, Feb 1987.

[12] Hans Kosina *et al.*, "Coupling of Monte Carlo and Drift Diffusion Method with Applications to Metal Oxide Semiconductor Field Effect Transistors," *Japanese Journal of Applied Physics*, vol. 29, no. 12A, p. L2283, 1990.

[13] M. Karner *et al.*, "Bringing physics to device design – A fast and predictive device simulation framework," in *Silicon Nanoelectronics Workshop (SNW)*, June 2015.